The State Scientific Center of Russia

The Budker Institute of Nuclear Physics

SB RAS

V.N. Baier, V.M. Katkov, V.M. Strakhovenko

ELECTROMAGNETIC SHOWERS IN CRYSTALS AT GeV ENERGIES

BudkerINP 95-15

НОВОСИБИРСК

Electromagnetic Showers in Crystals at GeV Energies

V.N.Baier, V.M.Katkov and V.M.Strakhovenko

The State Scientific Center of Russia
The Budker Institute of Nuclear Physics, SB RAS
630090, Novosibirsk, Russia

Abstract

Specific features of electromagnetic showers in crystals initiated by electrons with energies of a few GeV are considered, basing on a model form of radiation spectrum at axial alignment. Formulae describing the influence of ordered crystalline structure on incoherent processes are derived, using Yukawa potential for a separate atom. Positron yield from crystal and amorphous targets for the kinematics inherent in positron sources is calculated, showing definite advantages of crystals.

1 Introduction

Electron-photon showers in aligned single crystals have many distinctive features (see papers [1, 2]) as compared to amorphous media. First,the probability of photon emission from electrons and positrons as well as that of pair-production by photons depends rather sharply on the particle energy ε and on the direction of particle motion (angle of incidence θ_0) with respect to crystalline axes or planes. Secondly, effects in crystals are by several times or even by orders of magnitude stronger than in amorphous media. At sufficiently high energies expressions for these probabilities valid at any θ_0 were obtained in [3, 4]. Being the kernels of corresponding kinetic equations given in [2], the mentioned probabilities provide angular and energy dependence of shower characteristics which was confirmed experimentally in [5]. As it was noted in [6] these properties of the specific shower in crystals can be used to create detectors of high energy electrons(positrons) and photons with angular resolution better than $1\,mrad$ .In this paper we shall consider axial alignment when θ_0 with respect to the chosen axis is small as compared to the critical (Lindhard) angle $\theta_c = (2V_0/\varepsilon)^{1/2}$, where V_0 is a typical scale of the corresponding potential and ε is the particle energy, since in this case the most pronounced effects take place.

Kinetic equations describing the shower development were solved in [2] at some simplifying assumptions for the case when both the initial particle energy $\varepsilon_i(\omega_i)$ and the lower cut-off for registered particles $\varepsilon_f(\omega_f)$ are much larger than the characteristic value ω_{th} for which the probabilities of e^+e^- pair-production by a photon in the field of crystalline axes and in the corresponding amorphous medium are equal. We call it the hard cascade. In

this energy region one can use simplified expressions for the probabilities and entirely neglect the incoherent contribution to the shower development. In [2] the energy distributions of photons and charged particles were obtained in an analytical form allowing us to determine the optimal crystal thickness when the number of created particles is maximal for given cut-off value ε_f. For the intermediate case when $\varepsilon_i \gg \omega_{th}$, but $\varepsilon_f \leq \omega_{th}$ the Monte-Carlo simulation (MCS) procedure was used in [2] to evaluate the shower characteristics, while the probabilities were taken in so called constant field approximation (CFA) which corresponds to magnetic bremsshtrahlung approximation in description of photon emission. It should be noted that solutions of kinetic equations give shower characteristics averaged over large number of events and do not describe arising fluctuations. In this sense the description of shower development by computer simulation is more informative. On the other hand we always have to know averaged characteristics of shower, whereas within the MCS-method it requires a big statistic being more time-consuming.

In the present paper the soft cascade when $\varepsilon_{i,f} \ll \omega_{th}$ is investigated by means of MCS-method. More precisely, the showers initiated by electrons having energies of a few GeV will be considered. In this case the mechanism of photon emission owing to the regular motion of particles in the field of crystalline axes (coherent contribution) is dominant especially in the soft part of the spectrum, while the e^+e^- pair production is entirely due to the incoherent contribution (Bethe-Heitler mechanism) as in an amorphous matter.

In section 2 formulae are given used for description of basic processes in shower development simulation. In particular, we suggest a semi-phenomenological expression for the coherent contribution to the spectral distribution of the photon emission probability giving a satisfactory description in wide energy interval. In section 3 the obtained results and among them a possible use of crystalline targets in positron sources with a few GeV electrons are discussed.

2 Description of basic processes

While moving in a crystal, the initial and arising charged particles may emit photons and undergo multiple scattering and ionization energy loss. To describe these phenomena just as the pair-production process the most simplified expressions will be used in what follows, bearing in mind to derive a set of formulae enabling us to perform fast estimations of shower properties for different crystals, thicknesses and energies. At the same time, the accuracy

of calculations turns out to be quite admissible as it will be seen below.

Let us start with the coherent contribution to the radiation. As already mentioned, at sufficiently high energies corresponding expressions valid at any θ_0 were obtained in [4]. For $\theta_0 \ll V_0/m$ they reproduce CFA-limit. But even if the initial electron energy is high enough to apply mentioned description, charged particles arising in the course of a shower development may not satisfy this condition. In the case of a soft cascade we have to describe the radiation from these "soft" particles as well. Let us remind that within semi-classical theory of the QED-processes in any external field there are only two parameters: ρ and χ. The parameter ρ is a measure of the particle velocity deviation from a straight line in units of the natural emission angle $\gamma^{-1} = m/\varepsilon$, while the parameter χ being the ratio of the external field strength in the particle rest system to the critical QED-value $E_c = 1.32 \cdot 10^{16}$ eV/cm is responsible for the magnitude of quantum recoil effects. In crystals

$$\chi \sim \chi_s = V_0 \varepsilon / m^3 a_s ,$$

where a_s is the screening radius of a corresponding potential and

$$\rho \simeq (2V_0/m\theta_0)^2 \text{ for } \theta_0 > \theta_c \text{ and } \rho \simeq \rho_c = 2V_0\varepsilon/m^2 \text{ for } \eta_0 < \theta_c .$$

The values of a_s, V_0 and other parameters for different crystals are given in the Table of [4]. Let us remind also that at $\rho \ll 1$ the dipole approximation for a description of the radiation is valid and a typical formation time is $\sim \omega_0^{-1}$, where ω_0 is the characteristic frequency of motion. At $\rho \gg 1$ CFA is valid, the radiation formation time is $\sim \omega_0^{-1}\rho^{-1/2}$, i.e. much less than a period of motion. In this case the description of the emission process becomes local and we do not need to know what the particle trajectory is like contrary to the case of small $\rho \leq 1$ when we have to know it. If we now recollect that generally the two-dimensional problem of particle motion has not been solved yet in an analytical form, then evidently the same is true for the much more complicated problem of obtaining a radiation spectrum at such motion. We emphasize that for the coherent contribution to the total intensity of radiation $I_{ch}(\varepsilon)$ CFA gives a correct result up to very small energies when semi-classical approximation is still valid (see corresponding discussion in [4]).

There is a computer code [7] describing emission of photons from electrons moving in crystals which was applied to the investigation of soft cascades development as well [8]. This code includes the evaluation of the charged particle trajectory as an intermediate step in computation of the photon emission process. However, to obtain the reasonable statistic accuracy this

method is extremely time-consuming. The comparison has shown that our approach is faster by 2-3 orders of magnitude as that used in [8]. On the other hand, the latter has some advantages as more detailed description, in particular, it allows one to take into account different behavior of electrons and positrons in crystals. In the present paper it will be assumed that all charged particles initial and created are uniformly distributed over transverse (with respect to the corresponding axis) coordinates. Then the mentioned difference in e^+ and e^- behavior does not appear.

The known (see eq.(1.4) in [4]) estimate for the characteristic frequency of emitted photons ω at given frequency of motion ω_0 reads

$$u \equiv \frac{\omega}{\varepsilon - \omega} \simeq \frac{2\omega_0 \varepsilon}{m^2}(1+\rho)^{1/2}. \qquad (1)$$

Using also that $\omega_0 \sim \theta_0/a_s$, we suggest to describe the radiation from channeled and moving not very high above the potential barrier particles the following heuristic intensity spectrum:

$$\frac{dI_{ch}}{d\omega} = \frac{r(\varepsilon)\varepsilon}{u_0(\varepsilon)}\left[1+\frac{1}{(1+u)^2}\right]\left(\frac{u}{u_0}\right)^{1/3}\ln\left(\frac{u_0}{u}\right)\vartheta(u_0-u), \qquad (2)$$

where $\vartheta(z) = 1$ for $z > 0$ and $\vartheta(z) = 0$ for $z < 0$,

$$u_0 = \frac{25}{6}\chi_s + 80\frac{1}{ma_s}\frac{\sqrt{\rho_c}}{(2+\rho_c)}. \qquad (3)$$

The function $r(\varepsilon)$ in eq.(2) is determined by the condition of the coincidence of the total intensity

$$I_{ch}(\varepsilon) = \int_0^{\varepsilon} d\omega \left(\frac{dI_{ch}}{d\omega}\right)$$

given by eq.(2) with a corresponding expression obtained in CFA (see eq.(3.1) in [4]) for the uniform distribution over transverse coordinates. So eq.(2) reproduces the energy dependence of coherent contribution to the radiation length $L_{ch} = \varepsilon/I_{ch}(\varepsilon)$ inherent to CFA which as mentioned above is valid in a wide energy range.

The position of a maximum in the spectrum given by eq.(2) is always consistent with the estimate (1). For relatively small energies when $\rho_c \ll 1$ and correspondingly $u_0 \ll 1$, we can neglect the first term in the right-hand side of eq.(3) since $\rho_c/\chi_s = 2ma_s \gg 1$. In this case the spectrum (2) has a maximum at $\omega = \omega_{max} \simeq 0.05\varepsilon u_0 \simeq 2\varepsilon\sqrt{\rho_c}/(ma_s)$ which evidently coincides

in this (dipole) approximation with eq.(1). When $\rho_c \gg 1$ and CFA is valid the spectrum (2) reproduces not only the position of a maximum but also the shape of spectral distributions like those shown in Fig.2 of [4] obtained within the approximation mentioned. We have compared the shape of the spectrum (2) with available experimental data, but this procedure is somewhat indirect for several reasons. Sometimes very thin samples were used where the distribution of electrons over transverse coordinates was far from being uniform, sometimes energy loss spectra were measured which are noticeably different from true intensity spectra, sometimes emitted photons were collimated that also results in a change of the observed shape of spectra. Nevertheless, a qualitative agreement of the spectrum (2) with known experimental data holds for all energies beginning with $900\,MeV$. Of course, eq.(2) can not give a correct description of the coherent contribution to the radiation from particles with energies less than 100 MeV. Furthermore, multiple scattering is very intensified in this energy region so that particles may acquire an angle with respect to the axis noticeably exceeding θ_c. At the same time, for such energies the intensity $I_{ch}(\varepsilon)$ is already small as compared to that caused by the incoherent contribution $I_{br}(\varepsilon)$ which is always present in crystals in slightly modified form comparatively to the amorphous case. For instance, at $\varepsilon = 70$ MeV near $< 111 >$ axis of tungsten we have $I_{ch}/I_{br} \simeq 0.1$ and the coherent contribution can be simply neglected. Nevertheless, for the sake of consistency we shall use eq.(2) at any energy up to ε_f to describe the coherent contribution to the radiation. But for the particles acquiring an angle $\theta \geq \theta_c$ owing to multiple scattering, the quantity u_0 in eq.(3) will be multiplied by the factor $0.5\sqrt{1+(\theta/\theta_c)^2}$ according to eq.(1), since $\omega_0 \propto \theta$ at $\theta \geq \theta_c$.

Incoherent contribution to the radiation and pair-production probabilities was calculated in a standard way (see e.g. [9]) neglecting inelastic scattering on atomic electrons and therefore providing the accuracy of order of $1/Z$, where Z is the atomic number. For the sake of simplicity, Yukawa potential with a single screening radius $1/m\lambda$ was used giving the following form of the atomic form-factor

$$\frac{1-F(q)}{q^2} = \frac{1}{q^2+\lambda^2 m^2}, \qquad (4)$$

where $\lambda = Z^{1/3}/111$ was chosen to reproduce results obtained with the Molier potential in the case of a full screening.

In crystals the probabilities of incoherent processes acquire at given momentum transfer q the factor $R(q) = 1 - \exp(-q^2u_1^2)$, where u_1 is the one-dimensional thermal vibration amplitude of a lattice. A proof of this fact can be found in [10], where it was given in the first Born approximation for

the photon emission process. Taking the factor $R(q)$ into account and using eq.(4), we obtain for the incoherent contribution to the radiation intensity spectrum:

$$\frac{dI_{br}}{d\omega} = \frac{4Z^2\alpha^3 n}{m^2}\left\{\left[x^2+\frac{4}{3}(1-x)\right]g_1(S_\gamma)+\right.$$

$$\left.\left[x^2+2(1-x)\right]g_2(S_\gamma)-\frac{2}{3}(1-x)\,g_3(S_\gamma)\right\}, \qquad (5)$$

here $x=\omega/\varepsilon$, $\alpha=1/137$ is the fine structure constant, n is the density of atoms, $S_\gamma = mx/(1-x)/2\varepsilon\lambda$, λ was determined in eq.(4), and functions g_i are

$$g_1(y) = \ln(183/Z^{1/3}) - \frac{1}{42} - \xi^2\sum_{k=1}^{\infty}\frac{1}{k(k^2+\xi^2)} - 1 - \frac{1}{2}\ln(1+y^2) -$$

$$-\frac{1}{2}\int_{y^2}^{\infty}\frac{dt\,e^{-\mu^2 t}}{1+t}\,(1-\mu^2 t)\,;$$

$$g_2(y) = 1 - y\arctan\left(\frac{1}{y}\right) + \frac{y}{2}\int_{y^2}^{\infty}\frac{dt\,e^{-\mu^2 t}}{1+t}\left(\frac{1-2\mu^2 t}{\sqrt{t}}+\mu^2 y\right);$$

$$g_3(y) = \frac{5}{6} + 2y^2\left[1 - y\arctan\left(\frac{1}{y}\right) - \frac{3}{4}\ln\left(1+\frac{1}{y^2}\right)\right] +$$

$$+\frac{3}{2}\mu^2 y^2\int_{y^2}^{\infty}\frac{dt\,e^{-\mu^2 t}}{1+t}\left[1-\frac{4y}{3\sqrt{t}}+2\ln\left(\frac{y}{\sqrt{t}}\right)+\frac{1}{\mu^2 t}\left(1-\frac{2y}{3\sqrt{t}}\right)\right], \qquad (6)$$

where $\xi = Z\alpha$ and $\mu = u_1 m\lambda$. Note that the transition to the amorphous case in eq.(6) corresponds to the limit $\mu\to\infty(u_1\to\infty)$, when the terms containing integration over t vanish. At obtaining eq.(6), the factor $R(q)$ was taken into account only in the region of small momentum transfers $q \ll m$ since $u_1 m \gg 1$, while the contribution of large momentum transfers $q \geq m$ was not modified. Therefore the functions g_i do not tend to 0 when $\mu\to 0$. In fact, quantities μ are of order of unity, e.g. at room temperature $\mu = 0.49$ for tungsten and $\mu = 0.63$ for germanium. The argument S_γ of the functions g_i in eq.(5) is a product of the minimal momentum transfer and the effective screening radius of a potential so that the transition to the full screening case corresponds to the limit $S_\gamma\to 0$ ($y\to 0$ in eq.(6). In this limit we

obtain $g_2 = 1$, $g_3 = 5/6$ and the known expression (cf. eq.(18.30) in [9]) for amorphous matter is reproduced with only difference in the function g_1 where the correction connected with lattice vibrations survives.

The differential probability of the incoherent e^+e^--pair-production process is also expressed via the functions g_i, introduced in eq.(6):

$$\frac{dW_p}{dx} = \frac{4Z^2\alpha^3 n}{m^2}\left\{\left[1-\frac{4}{3}x(1-x)\right]g_1(S_p)+\right.$$

$$\left.\left[1-2x(1-x)\right]g_2(S_p)+\frac{2}{3}x(1-x)\,g_3(S_p)\right\}, \qquad (7)$$

where now $x=\varepsilon/\omega$, $S_p = m/[2x(1-x)\omega\lambda]$ and ε is the energy of one of the created particles.

Multiple scattering was described in the small-angle approximation by Gaussian distribution as in [11]. Using the atomic form-factor eq.(4), the magnitude of crystalline effects in multiple scattering connected with the arising factor $R(q)$ was estimated. For tungsten at room temperature, the width of angular distribution is diminished by 3 per cent as compared to amorphous value. Within the accepted accuracy these effects are ignored.

Ionization energy losses by fast electrons were described in terms of mean rate of energy loss per unit length, neglecting fluctuations:

$$\frac{d\varepsilon}{dl} = -\frac{\alpha\omega_p^2}{2}\left[\ln\left(\frac{2m\varepsilon}{\omega_p^2}\right)-2\right], \qquad (8)$$

here ω_p is the plasma frequency: $\omega_p^2 = 4\pi Z\alpha n/m$. According to [12], in eq.(8) the density effect correction which is due to the polarization of a medium by a charged particle is included. No specific crystal effects are taken into account in derivation of eq.(8), because the distribution over transverse coordinate as mentioned above was assumed to be uniform and the coherence itself can not appear owing to the inelastic character of the process under consideration. We have compared the quantity $d\varepsilon/dl$ from eq.(8) with the results for mean rate of energy loss by electrons and positrons given in [13] (see Fig.2 in [13] reproduced also in [11]). It turns out that very simple formula (8) is in agreement with the results of [13] for lead in the energy range $5\div 100$ MeV within an accuracy better than 10 per cent. Note yet that the transition to the so called restricted energy loss rate is realized if we change ε in the argument of ln in eq.(8) by ε_{max}, which is the maximal admissible energy transfer.

The formulae (2), (5), (7) and (8) constituting the basic set for our consideration were used in more or less standard MCS-procedure to obtain characteristics of the specific electron-photon shower in crystals for a few GeV energy region.

3 Discussion of results and conclusion

The contribution to any process going on in a crystal is a sum $Y = Y_{coh} + Y_{inc}$ where, generally speaking, the incoherent contribution Y_{inc} differs from the amorphous value Y_{am}. The scale of this modification depends on the process under consideration. For the total intensity of the incoherent radiation and the quantity $\tilde{L}_{rad} = \varepsilon / I_{br}$ connected to it, the typical scale of diminishing of I_{br} as compared to I_{am} at room temperature is depending on media 9 to 13 per cent. The diminishing of the total probability of pair-production is of the same order of magnitude. In particular, we obtain from eq.(5) for tungsten in the case of a full screening $\tilde{L}_{rad} = 1.1 L_{rad}$. As far as the coherent contribution to the pair-production probability is negligible in the considered energy region and modifications of incoherent contributions are small, distinctions in the soft cascade development in crystal and amorphous media are mainly due to the coherent contribution to the radiation. This contribution changes the shape of photon spectra, enriching their soft part and noticeably diminishing the effective radiation length L_{ef} determined by the relation

$$L_{ef}^{-1} = \tilde{L}_{rad}^{-1} + L_{ch}^{-1} .$$

So, for the $< 111 >$ axis of tungsten, we find $L_{ef} \simeq 0.13$ cm at $\varepsilon = 2$ GeV and $L_{ef} \simeq 0.08$ cm at $\varepsilon = 5$ GeV, which are several times less than the amorphous value $L_{rad} \simeq 0.35$ cm. Thus in a crystal the initial electron is converted into photons along appreciably shorter length than in a corresponding amorphous medium, while further development of the soft shower in both media is more or less the same. Hence the most pronounced distinctions of shower characteristics in the amorphous and crystal case appear for small thicknesses. It is clear that for the valuable use of crystal properties in the case of suggested (see e.g. [8]) target composed of crystal and amorphous layers, the former must be of a few L_{ef} thick.

The cut-off value $\varepsilon_f = 5$ MeV will be used in what follows and all the results obtained are normalized per one incident electron. In Fig.1 a part ($5 < \omega < 200$ MeV) of photon spectra generated in L_{rad} and $2L_{rad}$ thick amorphous and crystal tungsten are shown. For the sake of better visualization, the intensity spectra $\omega dN_\gamma / d\omega$ are plotted. For the thickness $L = L_{rad}$,

amorphous spectra (curves 1) have more or less standard shape and those from a crystal (curves 2) are approximately two and three times higher correspondingly for the initial energy ε_i of 3 and 5 GeV. For the thickness $L = 2L_{rad}$, the very soft part of all the spectra rises owing to the radiation from secondary e^+ and e^- having usually small energies. As the photon energy increases, distinctions between spectra obtained for different thicknesses decrease. In Fig.2 for the same conditions as in Fig.1 the energy distributions of created positrons are shown. We emphasize that within our approach the distributions of secondary electrons are the same as those of positrons. All the distributions presented in Fig.2 are peaked on the left edge and fall rapidly as the positron energy increases. The shape of curves differ weakly in amorphous and crystal cases and for different energies and thicknesses. For the chosen value $\varepsilon_f = 5$ MeV the number of positrons with $\varepsilon > \varepsilon_f$ in crystals achieves a maximum value at $L \simeq 3.5 L_{rad}$ which is shorter than in the amorphous case for reasons discussed above. It can be seen in Fig.3 where this number as well as the number of positrons with $\varepsilon < \varepsilon_f$ created in a crystal are plotted versus the crystal thickness.

To estimate the possibility of utilization of crystal targets in a positron source it is important to know not the total number of created positrons but the number of positrons in a definite phase space which can be accepted by the corresponding matching optical system. We shall use typical parameters of such system mentioned in [8], assuming that the energies of accepted positrons and their transverse (with respect to the incident beam direction) momenta must satisfy the following relation

$$5 \text{ MeV} \leq \varepsilon \leq 25 \text{ MeV} , \quad p_\perp \leq 4 \text{ MeV/c} .$$

The number of accepted positrons N_+^A depending on the initial electron energy, the thickness and type of crystals are presented in Figs. 4,5,6. It is seen that the maximal yield is achieved at $L \sim 4 L_{rad}$ and the maximal value is increasing as the atomic number Z increases. The latter property is connected with the fact that with increasing Z the number of additional photons emitted by the coherent mechanism increases as well. An enlargement of the transverse momentum boundary value leads naturally to an increase of the accepted positron number and vice versa, what is illustrated by Fig.7.

The energy deposited in a target by the initial electron and created charged particles is one of the fundamental characteristics of the positron source. The expression (8) gives an adequate description of the ionization energy losses by fast electrons and positrons but, strictly speaking, the energy deposited in a sample may be somewhat less than these losses. Therefore

our results for the dissipated energy must be considered as the upper bound. In Fig.8 both the accepted positron yield and the deposited energy per one incident electron are presented for amorphous and crystal tungsten depending on the target thickness. It is seen that the relative gain for a crystal increases with increasing energy of initial electrons. For given number of accepted positrons N_+^A, the energy deposited ε_{dep} in a crystal sample is less than in an amorphous one. It can be derived from Fig.8 but is more evident in Fig.9 where N_+^A versus ε_{dep} is plotted for crystal Si, Ge, W and amorphous W at $\varepsilon_i = 5$ GeV. Concerning crystal-amorphous ratio, the initial electron having a maximal ionization energy loss rate keeps its energy almost unchanged for a longer time in an amorphous target owing to smaller photon emission intensity. As far as this ratio in the crystal case, the same positron yield is achieved (if achieved at all) in different crystals for thicknesses comparable in units of their own radiation length $L_{rad} \propto Z^{-2}$ while mean rate of energy loss per unit length $dE/dl \propto Z$. So, for given value of N_+^A, the quantity ε_{dep} is larger for smaller Z as can be seen in Fig.9.

We have compared our results presented in Fig.7 with those obtained in [14] within approach of [8] for the maximal available in [14] thickness of $0.7cm$ crystal tungsten. It turns out that our results are rather close to those obtained in [14] but systematically lower what might be expected since the modification (diminishing) of incoherent contribution to photon emission and pair-production in a crystal is not taken into account within approach of [8]. In fact the difference in N_+^A magnitudes is between 20 and 6.4 per cent depending on the boundary $p_\perp$ value and it diminishes as $p_\perp$ increases.

The description developed and the results obtained in the present paper allows one, in particular, to optimize the parameters of a crystal based positron source. It is clear that in the energy range of a few GeV crystals with large atomic numbers Z have evident advantages. The number of accepted positrons of order of unity can be achieved at admissible magnitude of energy dissipation.

Acknowledgements. We express our gratitude for kind hospitality and valuable discussions during our stay in France to X.Artru and R.Chehab. We are indebted to the International Science Foundation supported in part this research by Grant N RP 6000.

References

[1] V.N.Baier, V.M.Katkov and V.M.Strakhovenko, Sov. Phys. Dokl. **30**, 474 (1986).

[2] V.N.Baier, V.M.Katkov and V.M.Strakhovenko, Nucl. Instr. and Meth. **B27**, 360 (1987).

[3] V.N.Baier, V.M.Katkov and V.M.Strakhovenko, Nucl. Instr. and Meth. **B16**, 5 (1986).

[4] V.N.Baier, V.M.Katkov and V.M.Strakhovenko, Sov. Phys. JETP **65**, 686 (1987).

[5] R.Medenwaldt, S.P.Moller, S.Tang-Petersen et al., Phys. Lett. **B227**, 483 (1989).

[6] V.N.Baier, V.M.Katkov and V.M.Strakhovenko, Nucl. Instr. and Meth. **A250**, 514 (1986).

[7] X.Artru, Nucl. Instr. and Meth. **B48**, 278 (1990).

[8] X.Artru, V.N.Baier, R.Chehab, A.Jejcic, Nucl. Instr. and Meth. **A344**, 443 (1994).

[9] V.N.Baier, V.M.Katkov and V.S.Fadin. Radiation from Relativistic Electrons (in Russian). Atomizdat. Moscow, 1973.

[10] M.L.Ter-Mikaelyan. High-Energy Electromagnetic Processes in Condensed Media. Wiley-Interscience, New York, 1972.

[11] Review of Particle Properties, Phys. Rev.**D50**, Part 1, pp. 1253, 1260 (1994).

[12] R.M.Sternheimer, Phys.Rev. **145**, 247 (1966).

[13] Messel and Crawford. Electron-Photon Shower Distribution Function Tables for Lead, Copper and Air Absorbers. Pergamon Press, 1970.

[14] T.V.Baier, private communication, 1994.

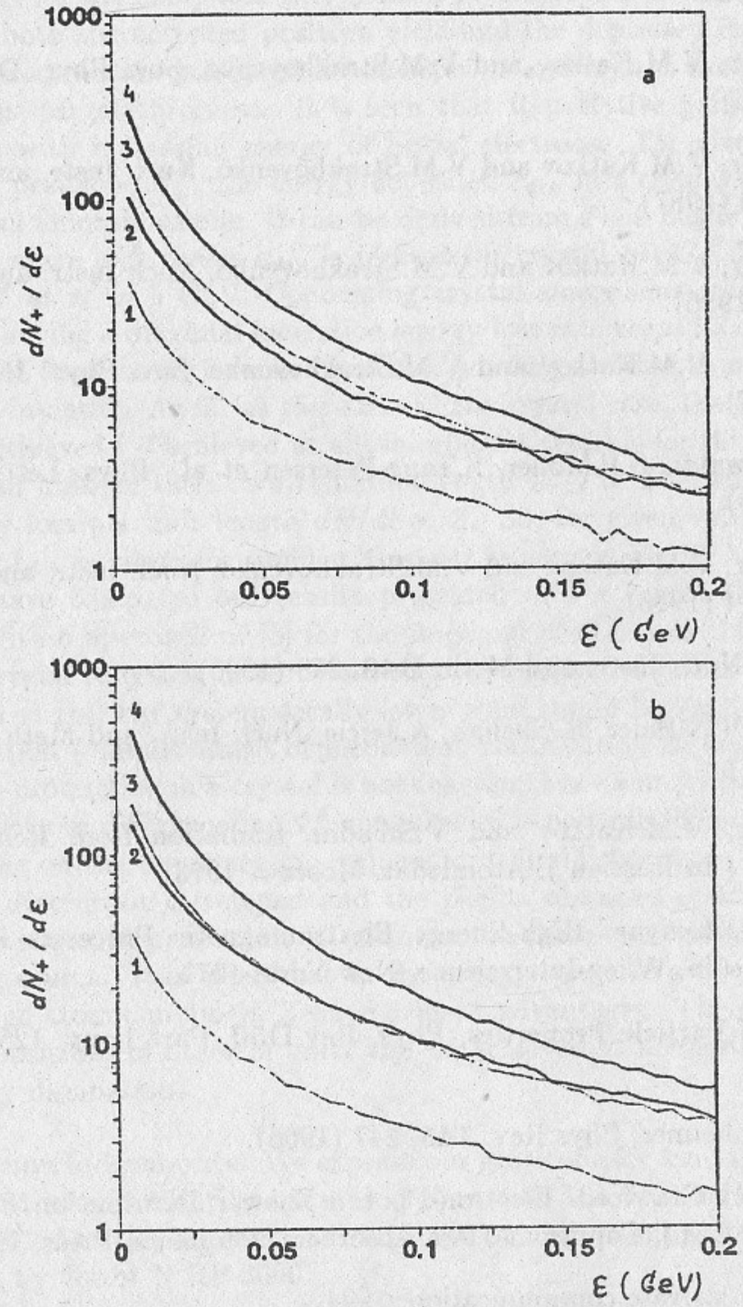

Fig. 1. Photon intensity spectra $\omega\, dN_\gamma/d\omega$ versus photon energy ω for $\varepsilon_i = 3$ GeV (a) and $\varepsilon_i = 5$ GeV (b) in amorphous (curves 1,3) and crystal (curves 2,4) tungsten near $< 111 >$-axis. The thickness is $L = 0.35$ cm (curves 1,2) and $L = 0.7$ cm (curves 3,4).

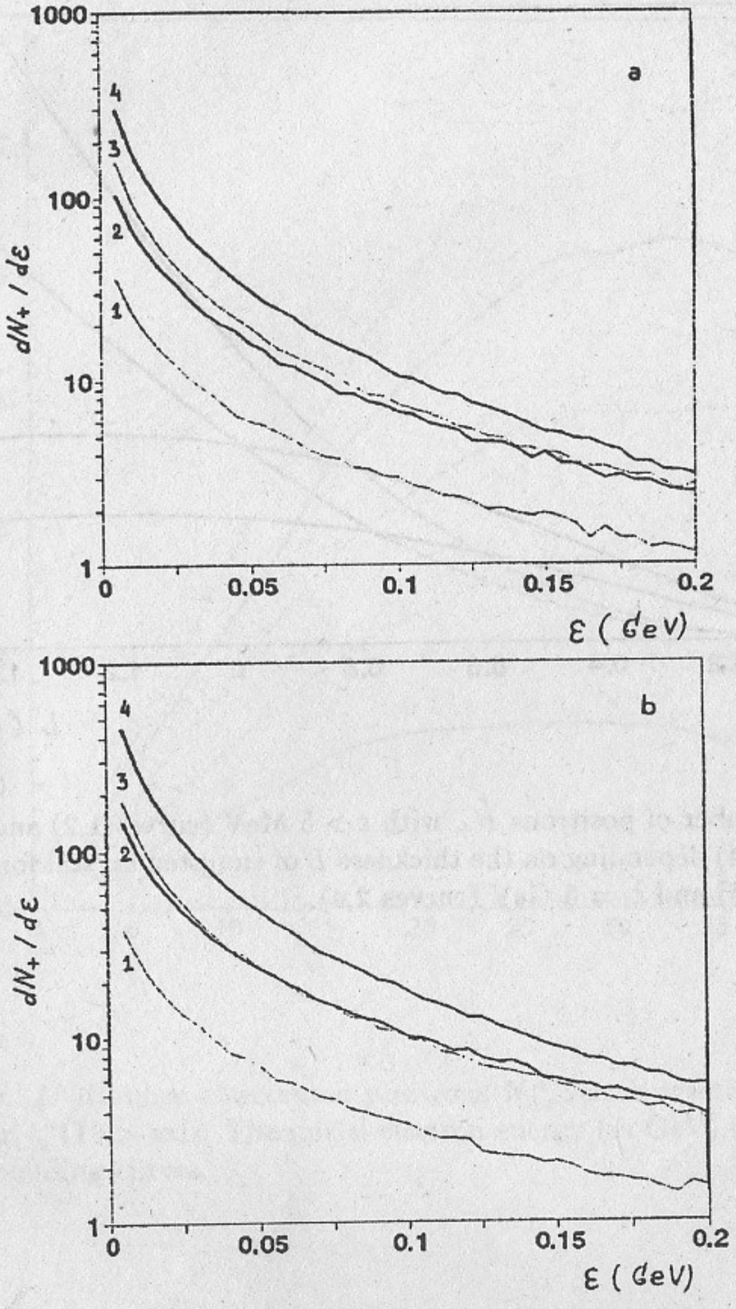

Fig. 2. Positron spectra $dN_+/d\varepsilon$ depending on positron energy ε for $\varepsilon_i = 3$ GeV (a) and $\varepsilon_i = 5$ GeV (b). Curves are labeled as in Fig.1.

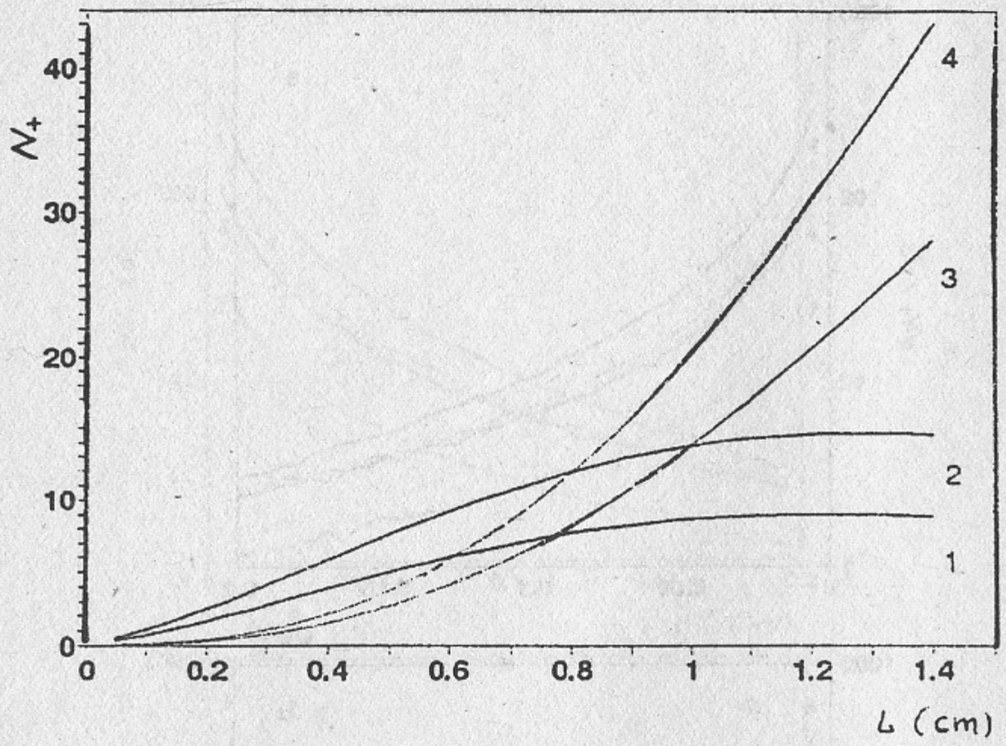

Fig. 3. Number of positrons N_+ with $\varepsilon > 5$ MeV (curves 1,2) and $\varepsilon < 5$ MeV (curves 3,4) depending on the thickness L of tungsten crystal for $\varepsilon_i = 3$ GeV (curves 1,3) and $\varepsilon_i = 5$ GeV (curves 2,4).

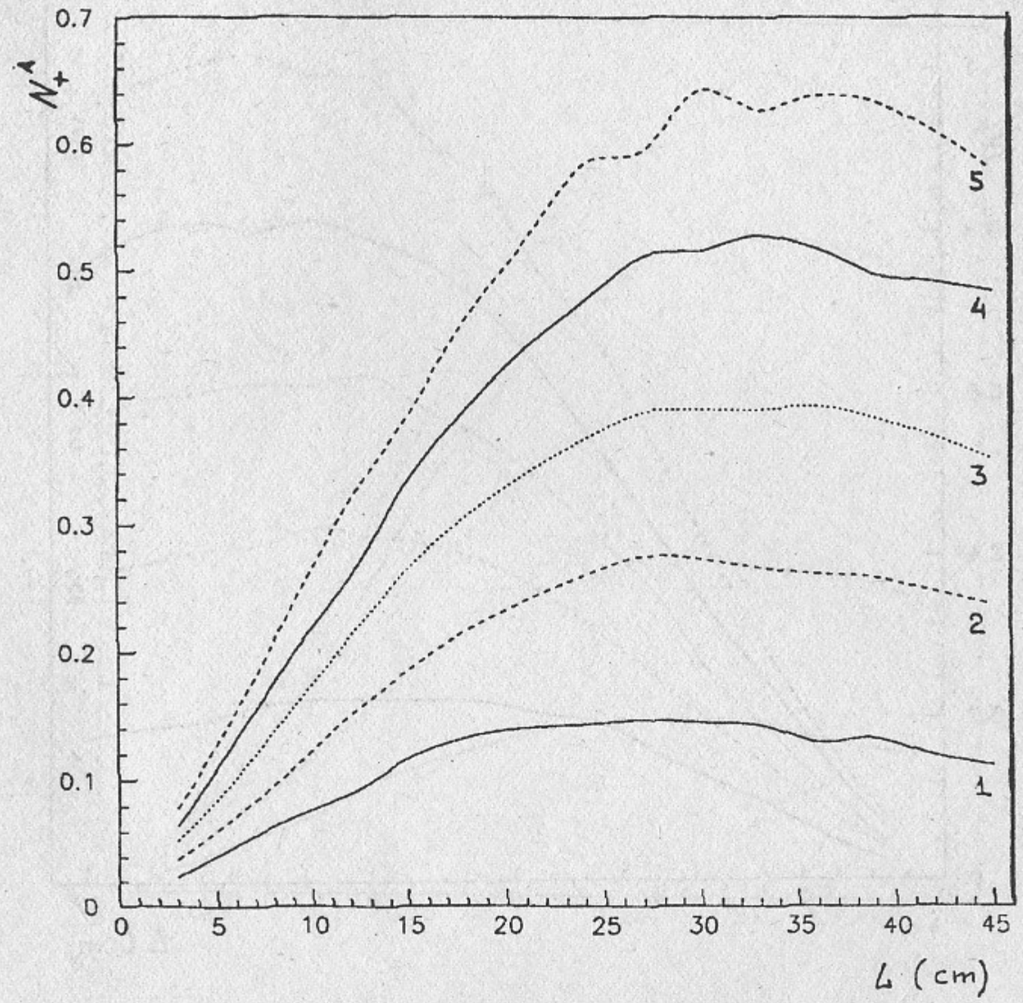

Fig. 4. Number of accepted positrons N_+^A versus crystal thickness L in *Si* near $< 110 >$-axis. The initial electron energy (in GeV) is indicated near corresponding curves.

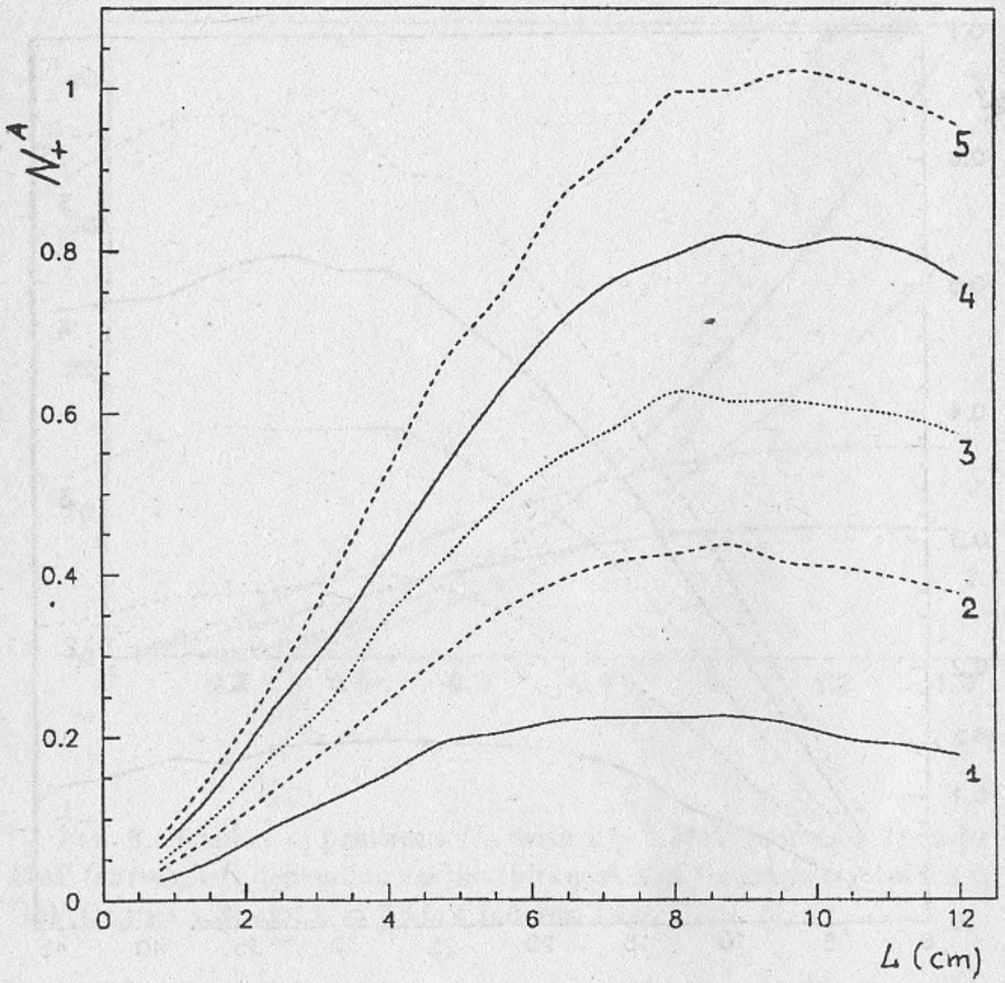

Fig. 5. The same as in Fig.4 but for Ge near $< 110 >$-axis .

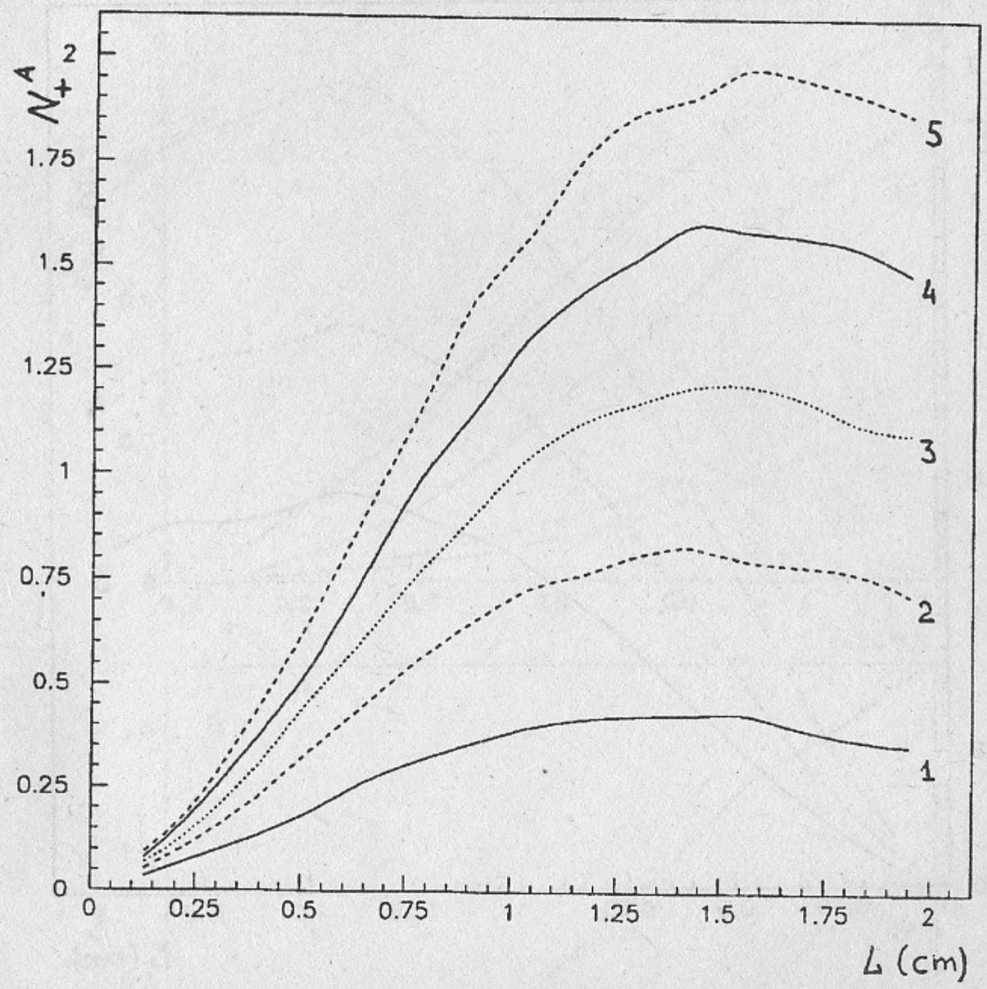

Fig. 6. The same as in Fig.4 but for W near $< 111 >$-axis.

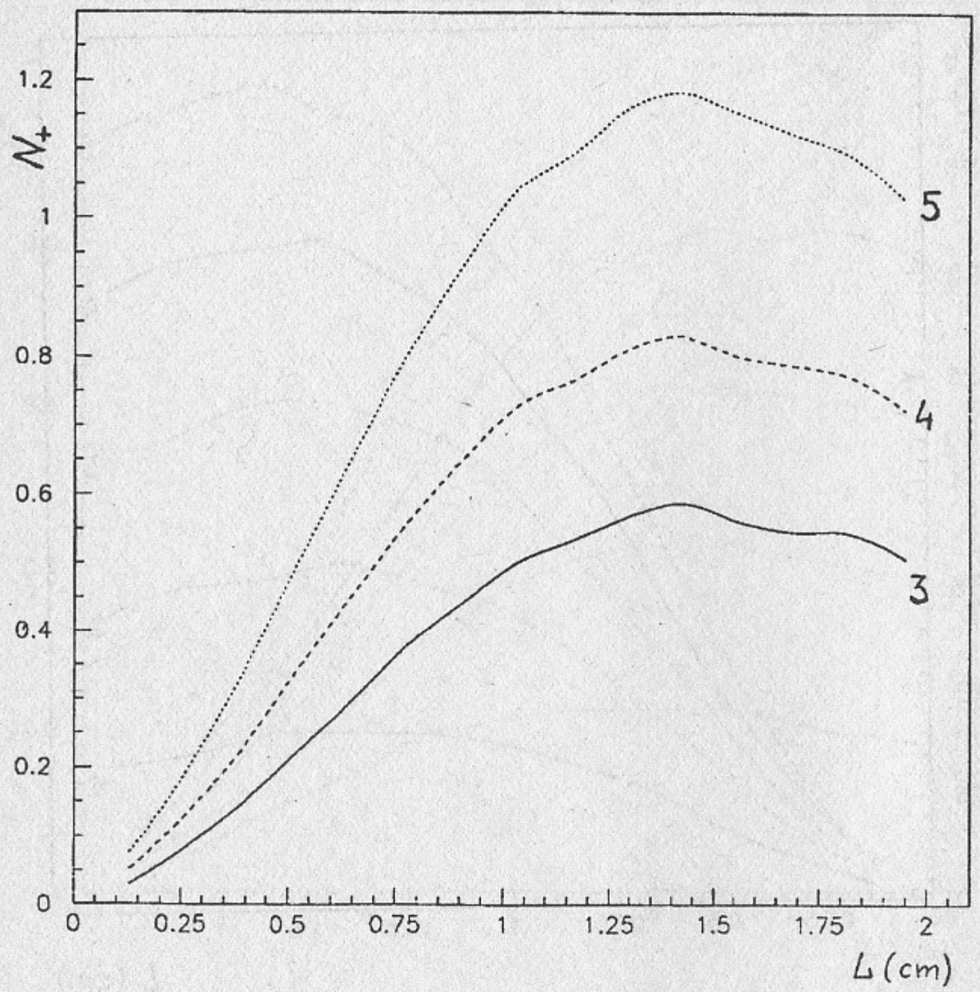

Fig. 7. Number of positrons having energies in the interval $5 \div 25$ MeV versus thickness of tungsten crystal for different values of boundary transverse momentum $p_\perp$ indicated (in MeV/c) near corresponding curves.

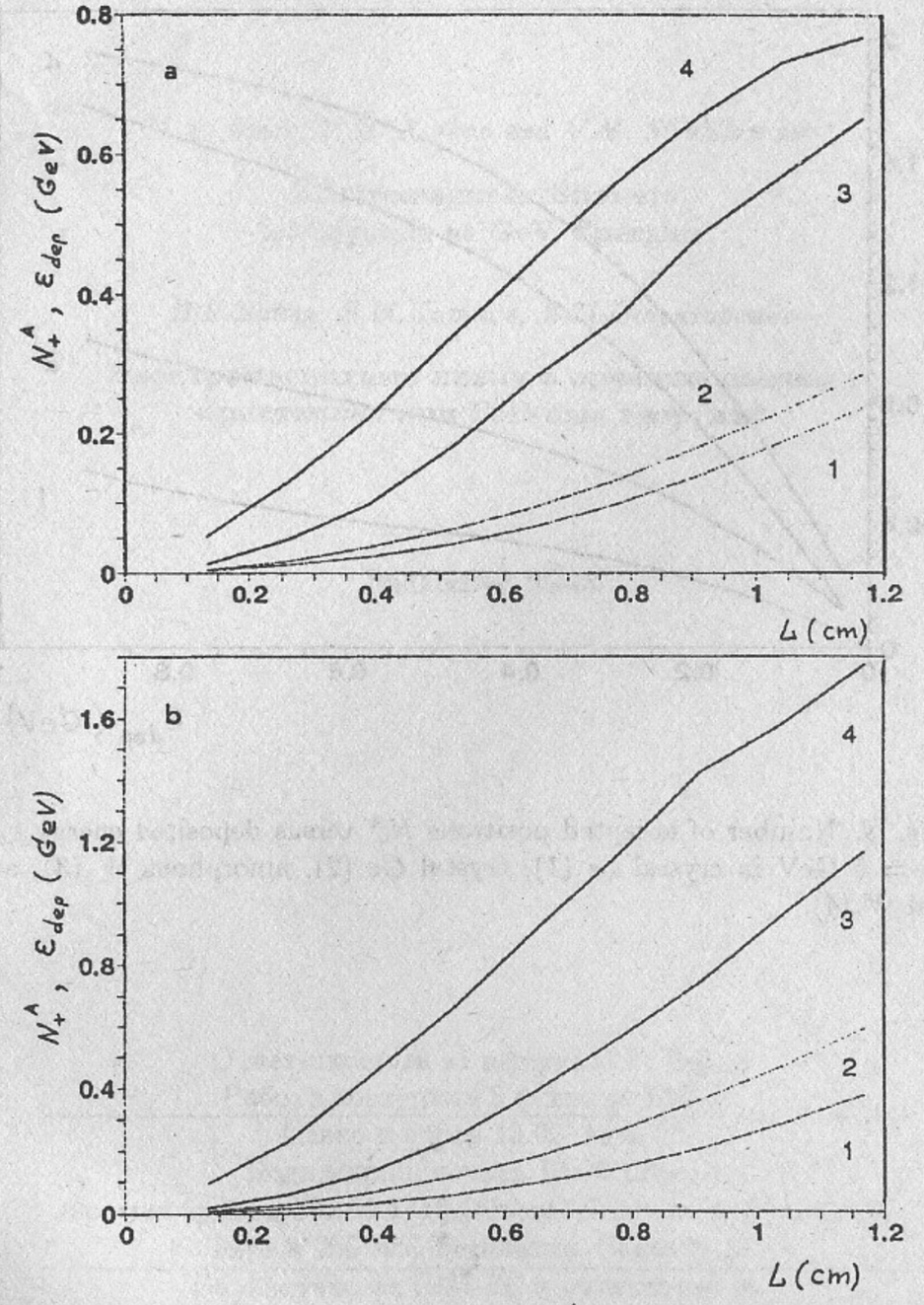

Fig. 8. Number of accepted positrons N_+^A (curves 3,4) and deposited energy ε_{dep} (curves 1,2) for $\varepsilon_i = 2$ GeV (a) and $\varepsilon_i = 5$ GeV (b) in amorphous (curves 1,3) and crystal (curves 2,4) tungsten depending on the thickness L.

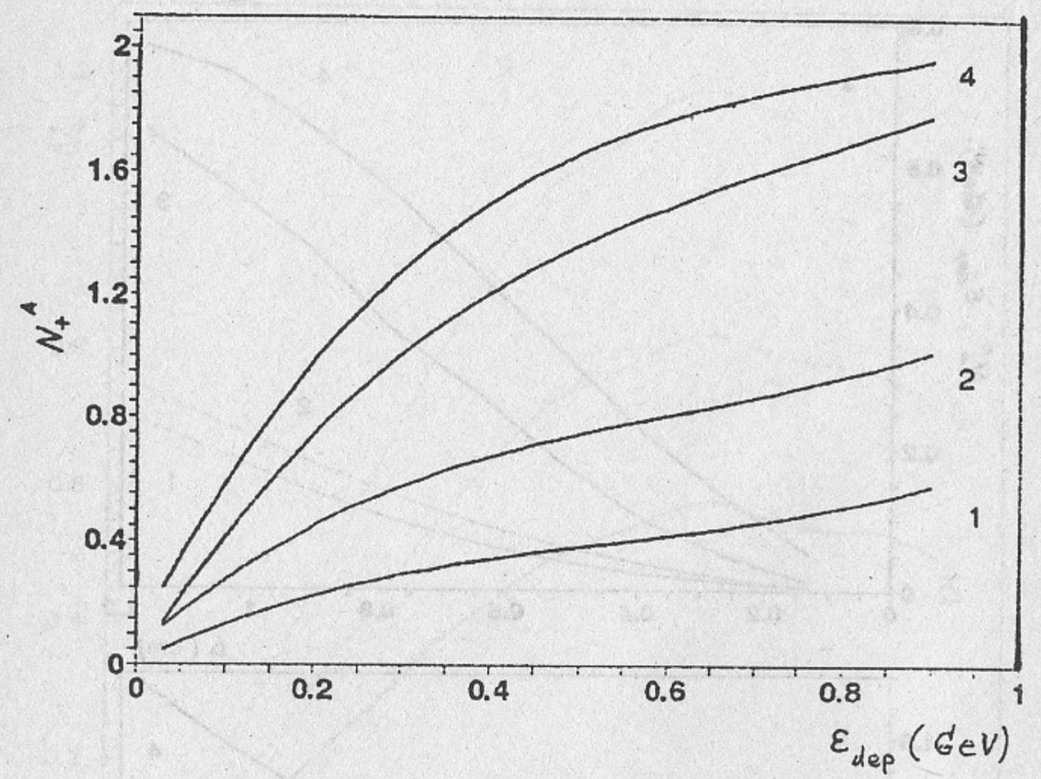

Fig. 9. Number of accepted positrons N_+^A versus deposited energy ε_{dep} for $\varepsilon_i = 5$ GeV in crystal *Si* (1), crystal *Ge* (2), amorphous *W* (3), and crystal *W* (4).

V.N. Baier, V.M. Katkov and V.M. Strakhovenko

Electromagnetic Showers in Crystals at GeV Energies

В.Н.Байер, В.М.Катков, В.М.Страховенко

Электромагнитные ливни в ориентированных кристаллах при ГэВ-ных энергиях

BudkerINP 95-15

Ответственный за выпуск С.Г. Попов
Работа поступила 8 февраля 1995 г.

Сдано в набор 13.02. 1995 г.
Подписано в печать 13.02 1995 г.
Формат бумаги 60×90 1/16 Объем 1,7 печ.л., 1,4 уч.-изд.л.
Тираж 200 экз. Бесплатно. Заказ N 15

Обработано на IBM PC и отпечатано на
ротапринте ГНЦ РФ "ИЯФ им. Г.И. Будкера СО РАН",
Новосибирск, 630090, пр. академика Лаврентьева, 11.